

The Effect of Magnetic Field on the Performance of Low-Power Cylindrical Hall Thrusters

IEPC-2005-099

*Presented at the 29th International Electric Propulsion Conference, Princeton University,
October 31 – November 4, 2005*

Artem Smirnov^{*}, Yevgeny Raitses[†], and Nathaniel J. Fisch[‡]

Princeton University Plasma Physics Laboratory, P. O. Box 451, Princeton, New Jersey 08543

Abstract: The annular design of the conventional Hall thruster does not naturally lend itself to scaling to low power. The efficiency tends to be lower, and the lifetime issues are more aggravated. Cylindrical geometry Hall thrusters have lower surface-to-volume ratio than conventional annular thrusters and, thus, seem to be more promising for scaling down. The effect of the magnetic field on the discharge characteristics and efficiency of the low-power cylindrical Hall thrusters with channel outer diameters of 2.6 cm and 3 cm was investigated. The thrust measurements were conducted at the Electric Propulsion and Plasma Dynamics Laboratory (EPPDyL, Princeton University). The thrust stand operation at low applied thrust and the accuracy of thrust measurements were studied in detail through the comparison of several calibration and measurement techniques. To achieve a sufficient accuracy of measurements, special calibration and measurement procedures were developed. The experimental results demonstrate that the enhancement of the axial component of the magnetic field in the cylindrical thruster leads to the increase of the thruster efficiency. A substantial flexibility in the magnetic field configuration of the cylindrical thruster is a key tool in achieving the high-efficiency operation. The electron confinement and ion acceleration can be optimized over a family of realizable magnetic field distributions.

I. Introduction

Scaling to low-power Hall thrusters requires the magnetic field to be increased inversely with length, as the thruster channel size is decreased.¹ The conventional (annular) Hall thrusters become inefficient when scaled to small sizes² because of the large surface-to-volume ratio and the difficulty in miniaturizing the magnetic circuit. Also, erosion of the walls of a small annular channel can severely limit the thruster lifetime. An alternative approach, which may be more suitable for scaling to low power, is a cylindrical Hall thruster (CHT) shown in Fig. 1. The CHTs have been studied both experimentally and theoretically and described in detail elsewhere.³⁻⁷ Currently existing CHTs, operated in the kilowatt and 100-Watt power ranges, exhibit performance comparable with conventional annular Hall thrusters of the similar size. Ion acceleration in CHTs occurs mainly in the cylindrical part of the channel and beyond the thruster exit. Therefore, CHTs, having lower surface-to-volume ratio as compared with conventional Hall thrusters, should suffer lower erosion of the channel walls and have a longer lifetime.

The stronger the electron transport to the anode is suppressed by the applied magnetic field, the larger the Hall thruster efficiency is.¹ The axial electron current in a CHT can be reduced by the magnetic field with an enhanced radial component and/or by the strong magnetic mirror in the cylindrical part of the channel. Plasma probe

^{*} Graduate Student, Program in Plasma Physics, Princeton University, asmirnov@princeton.edu.

[†] Research Physicist, Princeton Plasma Physics Laboratory, yraitses@pppl.gov.

[‡] Professor, Department of Astrophysical Sciences, Princeton University, fisch@pppl.gov.

measurements⁶ showed that, in fact, most of the potential drop is localized in the cylindrical part of the channel [see Fig. 1(a)], which implies that most of the resistance to the axial electron flow is generated by the divergent magnetic field lines.

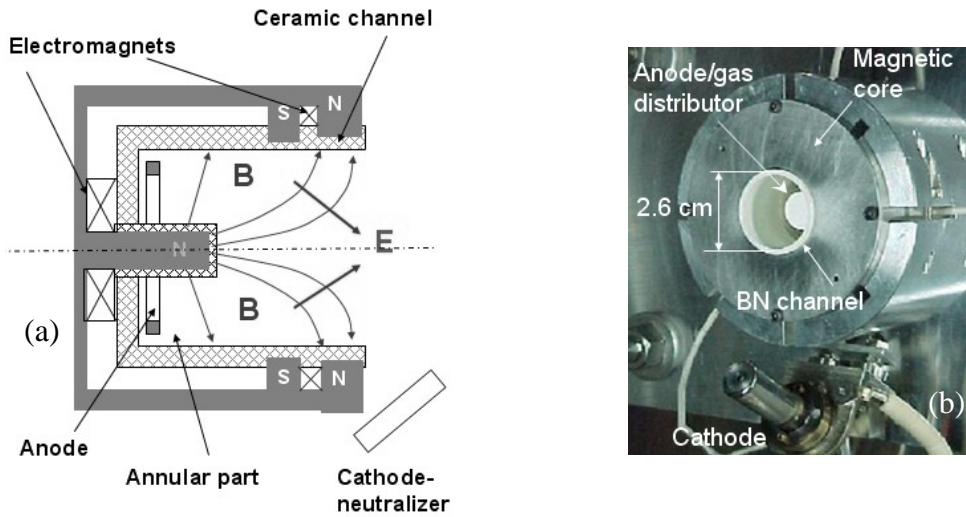


Fig. 1. (a) Schematic of a cylindrical Hall thruster. (b) The 2.6 cm cylindrical Hall thruster.

In contrast to the conventional annular geometry, in the cylindrical geometry the axial potential distribution is critical for electron confinement. This is because there is now a large axial gradient to the magnetic field over the cylindrical part of the channel, which means that electrons drift outwards through the $\mu_e \nabla B$ force, even as they drift azimuthally around the cylinder axis. In the absence of an axial potential, the electrons would simply mirror out of the region of high magnetic field. The axial potential that accelerates ions outwards, now also plays an important role in confining electrons within the thruster.

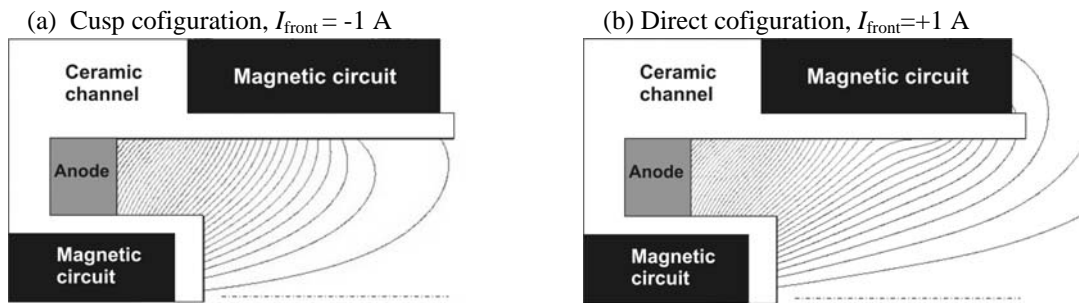


Fig. 2. The magnetic field distribution in the channel of the 2.6 cm CHT in the cusp (a) and direct (b) configurations. The current in the back coil is fixed ($I_{back} > 0$). Note that the variation of I_{front} alters the magnetic field distribution in the annular part of the channel insignificantly.

The variation of the current in the back magnetic coil of the CHT mainly changes the magnetic field magnitude without altering the shape of magnetic field surfaces. It is generally observed that the increase of the back coil current leads to the monotonic decrease of the discharge current. The variation of the front coil current changes the magnetic field distribution as shown in Fig. 2, with the most pronounced changes occurring in the cylindrical part of the channel. When the current in the front coil is counter-directed to that in the back coil [$I_{front} < 0$, Fig. 2(a)], the “cusp” magnetic field with an enhanced radial component is created. Swapping the polarity of the front coil current ($I_{front} > 0$) leads to the enhancement of the axial component of the magnetic field and generation of a stronger magnetic mirror near the thruster axis. This “direct” configuration of the magnetic field is shown in Fig. 2(b).

Now, ions are accelerated primarily in the direction perpendicular to the magnetic field surfaces, away from the channel walls. Therefore, there is a trade-off between the amount of the ion wall losses and the ion momentum

fraction that contributes to the thrust. By varying the current in the front coil we can, thus, control not only electron transport to the anode, but also ion creation and acceleration.⁸

In the present work, we studied two cylindrical thrusters, namely, the 2.6-cm-diameter CHT and its modification with the channel outer diameter of 3 cm. The goal of the present work was to explore the effect of the magnetic field configuration on the thruster performance. In particular, the dependence of the discharge current, generated thrust, and thruster efficiency on the current in the front magnetic coil was investigated. It is our further objective to understand how the ion acceleration and magnetic insulation of the discharge can be optimized by varying the geometry and strength of the thruster magnetic field.

The Electric Propulsion and Plasma Dynamics Laboratory (EPPDyL, Princeton University) thrust stand was used for the thrust measurements. This thrust stand was designed to accurately measure impulse bits of pulsed plasma thrusters.⁹ It was also predicted to be capable of measuring low steady state thrust, as low as 20 μN . In the present work, the thrust stand operation at low applied thrust and the accuracy of thrust measurements were investigated in detail through the comparison of several calibration and measurement techniques. To decrease the experimental uncertainty, special calibration and measurement procedures were developed.

This paper is organized as follows: In Sec II, the fundamentals of thrust stand operation are outlined. Section III gives a brief description of the thrust stand calibration procedures. In Sec. IV, the experimental procedure is described and the subtleties of the thrust measurements are analyzed. We present the key experimental results and discuss their implications in Sec. V. In Sec. VI, we summarize our main conclusions.

II. Fundamentals of thrust stand operation

The thrust stand schematic and photo are shown in Fig. 3. The thruster was mounted on a swinging arm that could rotate around a vertical axis. The restoring force, proportional to the arm displacement from an equilibrium position, was due to the torsion in the flexural pivots, as well as strain in the thruster wiring and the flexible silicon gas line, which connected the thruster with the rigid part of the thrust stand. The arm position was recorded by measuring the signal of the linear variable differential transformer (LVDT). The LVDT signal is directly proportional to the arm displacement.

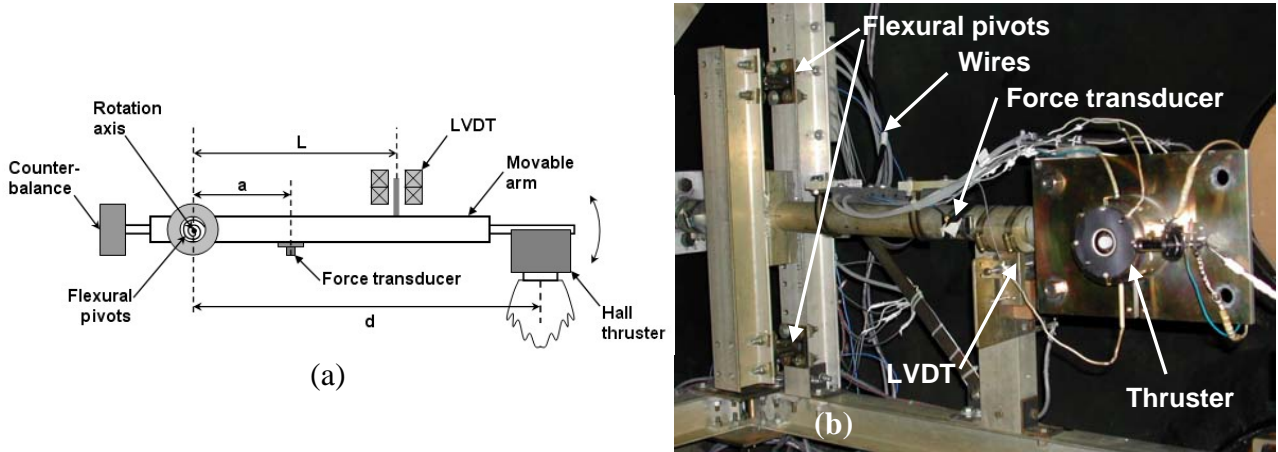


Fig. 3. (a) Schematic of the thrust stand setup, top view. (b) Thrust stand with the 2.6 cm cylindrical Hall thruster mounted on it.

The thrust stand dynamics can be described, quite accurately, by the damped linear oscillator equation, which corresponds to a simple spring-mass system:

$$\ddot{x} + 2\gamma\dot{x} + \omega_0^2(x - x_0) = \frac{F(t)}{m_{\text{eff}}}, \quad (1)$$

where γ is the damping coefficient, ω_0 is the natural frequency, $F(t)$ is the thrust generated by the thruster, x_0 is the equilibrium position, and m_{eff} is the effective mass, which is determined by the moment of inertia M of the thrust

arm with the thruster mounted on it:

$$m_{\text{eff}} = \frac{M}{Ld}. \quad (2)$$

Here, L and d are the distances from the rotation axis to the LVDT and thruster axis, respectively [see Fig. 3(a)]. The natural frequency depends on the effective mass and the effective spring constant k_{eff} as

$$\omega_0 = \sqrt{\frac{k_{\text{eff}}}{m_{\text{eff}}}}. \quad (3)$$

The steady-state thrust can, in principle, be determined from Eq. (1) as

$$F = k_{\text{eff}}(x - x_0). \quad (4)$$

In the present setup it is impossible to eliminate the contribution of the wires and the gas line to the effective spring constant. Although experimentally minimized, this contribution was of the order of the torsional spring constant of the flexural pivots. This fact has two important practical implications. First, after the thruster assembling or any change done to the wiring, the thrust stand has to be calibrated. Second, due to the wire heating during the thruster operation, the effective spring constant changes slightly with time and, therefore, the measurement procedure should be designed so that to determine the “instantaneous” value of k_{eff} . Yet another experimental complication is the observed long-timescale equilibrium position drift, which is brought about by (i) the vacuum tank vibration caused by the operation of the mechanical pumps and (ii) thrust stand heating due to the thruster operation. Thus, to accurately determine the thrust, the instantaneous values of x_0 and k_{eff} must be obtained during a measurement.

III. Thrust stand calibration

A. Primary calibration procedure

As opposed to the equilibrium position and the effective spring constant, the effective mass changes insignificantly during the thruster operation. Indeed, the clearance ΔL between the movable inner rod of LVDT and the LVDT magnetic coils, which are mounted rigidly on the thrust stand frame, is about 1 mm only. The distance between the rotation axis and the LVDT rod L [see Fig. 3(a)] is 49.5 cm. The LVDT rod sticking inside the coils was never observed during the operation. Therefore, the maximum relative deviation of the moment of inertia, which could be potentially caused by tilting or thermal expansion of the thrust stand arm, is definitely less than about $2\Delta L/L \sim 0.5\%$. As shown at the end of this section, this possible variation is a few times smaller than the experimental uncertainty of m_{eff} calibration.

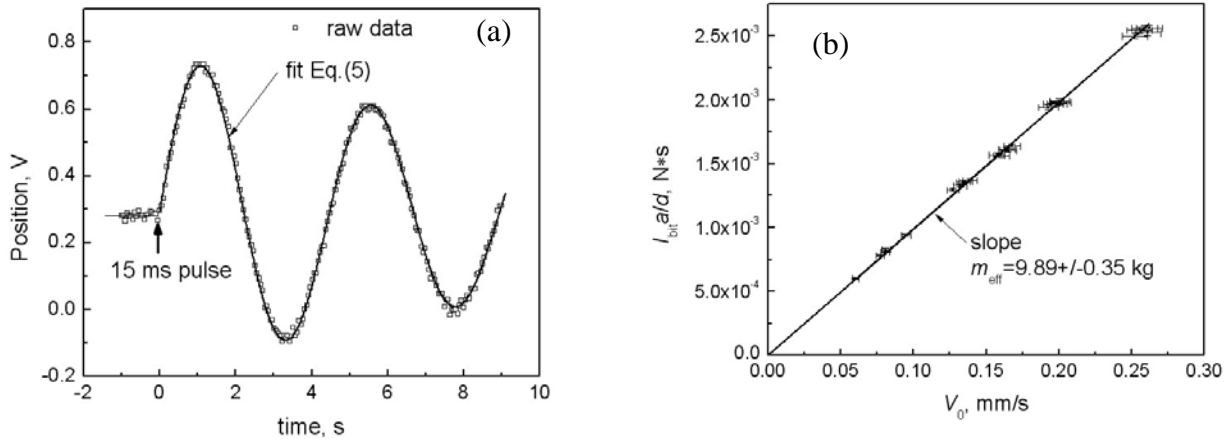


Fig. 4. (a) Thrust arm position versus time after the calibrating pendulum strike at $t=0$. Solid line shows the result of fitting the data with the damped linear oscillator response function, Eq. (5). (b) Linear dependence of $I_{\text{bit}}a/d$ on V_0 , with m_{eff} being the slope of the line.

The standard calibration procedure for the EPPDyL thrust stand was thoroughly described elsewhere [8]. The idea of this procedure is to observe the dynamic response of the thrust stand arm to the applied impulse bit I_{bit} . If the arm is initially at rest and the duration of the impulse bit is much less than the natural period of oscillations, then the arm response is

$$x(t) = x_0 + \frac{V_0}{\omega} \sin(\omega t) \exp(-\gamma t), \quad (5)$$

where $\omega = \sqrt{\omega_0^2 - \gamma^2}$ and V_0 is the velocity increment due to I_{bit} . In practice, the impulse bit is delivered by a small calibrating pendulum that strikes the force transducer mounted on the arm [see Fig. 3(a)]. The force transducer output signal is integrated to obtain the total impulse $I_{\text{bit}} = \int F(t) dt$, while the LVDT signal $x(t)$ is recorded and fitted numerically with response function (5) in order to determine V_0 , ω , and γ . The data curve fitting was performed using Origin software package. As shown in Fig. 4(a), the calibration data can be fitted with the damped linear oscillator response function with a high degree of accuracy. From Eq. (1), V_0 is related to I_{bit} as

$$V_0 = \frac{I_{\text{bit}} a}{m_{\text{eff}} d}. \quad (6)$$

Therefore, the dependence of quantity $I_{\text{bit}}a/d$ on V_0 is linear, and m_{eff} is the slope of the straight line, as shown in Fig. 4(b). Having determined m_{eff} , ω , and γ , we calculate the effective spring constant as

$$k_{\text{eff}} = (\omega^2 + \gamma^2) m_{\text{eff}}. \quad (7)$$

There are several sources of uncertainty in the calibration of m_{eff} [see Eq. (6)]. The uncertainty in I_{bit} , which is due primarily to the offset in the zero level of the recorded force $F(t)$ before and after the pulse, is estimated to be about $\pm 0.5\%$. The error in V_0 measurement is caused mainly by the scatter of the data around the fit line. If the data scatter is considered to be noise, a standard deviation of the line slope near $t=0$ [see Fig. 4(a)] can be calculated. This standard deviation is about 1% of V_0 . However, there are some inherent constraints of the fitting procedure based on Eq. (5). To investigate a possible error associated with the fitting procedure, we compared the values of V_0 obtained by the method described above with those derived from the linear fit to the position data after the pulse. Varying the time interval over which the linear fit is done, we found that the discrepancy between the values of V_0 calculated by different methods was always less than about $\pm 2.5\%$ of V_0 . This value seems to be a reasonable estimate of the uncertainty in V_0 measurement. Finally, distances a and d were measured with errors about ± 1 mm, which made the relative uncertainties $\Delta a/a$ and $\Delta d/d$ equal to about $\pm 0.25\%$ and $\pm 0.15\%$, respectively. Using the error propagation formula,¹⁰ we find the total relative uncertainty of m_{eff} measurement to be about $\pm 2.6\%$.

B. Supplementary calibration procedure

As will be shown in Sec. IV A, some features of the thrust stand behavior during the measurements suggest that an additional independent thrust stand calibration procedure, which, preferably, does not rely on the momentum transfer from the calibrating pendulum to the thrust stand arm, is required for a cross-check. We developed a supplementary calibration procedure based on varying the moment of inertia of the arm and monitoring the corresponding changes in the natural frequency of oscillations. Namely, if the moment of inertia gets increment ΔM and all other thrust stand parameters are kept the same, then, as follows from Eqs. (2-3), the shift in the natural frequency is such that

$$\frac{\Delta M}{Ld} = k_{\text{eff}} \Delta \left(\frac{1}{\omega_0^2} \right). \quad (8)$$

In practice, a few steel discs with known moments of inertia were added sequentially to the counterbalance of the thrust stand [see Fig. 3(a)]. Upon adding a new weight, we determined a new value of the natural frequency by fitting a sample trace of position versus time with the damped sinusoidal function. Then, by plotting quantity $\Delta M/(Ld)$ versus ω_0^{-2} we found the best-fit value of the effective spring constant k_{eff} (Fig. 5). Finally, by applying Eq. (2), the effective mass of the thrust arm with the unloaded counterbalance, $m_{\text{eff}}=9.00$ kg, was determined.

The supplementary calibration procedure was not optimized for high accuracy and the uncertainty of m_{eff} determination by this method, $\Delta m_{\text{eff}}/m_{\text{eff}} \sim -13\% / +26\%$, is a few times larger than that of the primary calibration. However, the approximate value of m_{eff} , obtained in the supplementary calibration, is only about 9% smaller than the one from the primary calibration. Thus, there seems to be a reasonable agreement between the results of different calibrations.

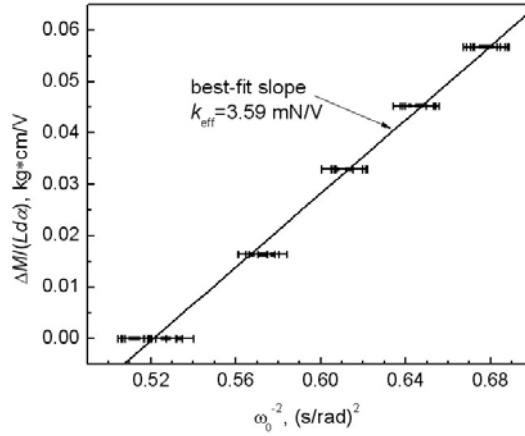


Fig. 5. The measured dependence of quantity $\Delta M/(Ld\alpha)$ on ω_0^{-2} . Here, α is the coefficient of linearity between the actual arm displacement in millimeters and the LVDT signal in Volts. Coefficient α should be added to the denominator of the left hand side of Eq. (8) in order to have k_{eff} expressed in its practical unit, mN/V. The slope of the best-fit straight line is k_{eff} .

IV. Experimental procedure

A. Measurement method

In order to accurately measure thrust, the following procedure for determining the instantaneous equilibrium position and effective spring constant was developed. Once the steady-state operation of the thruster was achieved (in about half hour from the ignition of the discharge), the discharge voltage, the coil power, and the gas flow to the anode and cathode were turned off, and oscillations of the thrust arm position $x(t)$ were recorded (Fig. 6). The steady state thrust arm position x_s , corresponding to the firing thruster, was determined from averaging $x(t)$ over a two-second interval immediately before turning the thruster off. The instantaneous equilibrium position x_0 together with ω_0 were determined from fitting a few periods of oscillations, starting from the first minimum $x_{\text{min}1}$ of $x(t)$, with the damped linear oscillator response function

$$x(t) = x_0 + A \sin(\omega(t - \tau)) \exp(-\gamma(t - \tau)). \quad (9)$$

Combining instantaneous (on a generally rather slow time scale of the thrust stand parameter drift) $\omega_0 = \sqrt{\omega^2 + \gamma^2}$ with m_{eff} found in the calibration, we derive the instantaneous effective spring constant.

Within the framework of this fitting procedure, varying the number of periods, over which the data fit is performed, as well as choosing different start point $x' > x_{\min 1}$ of the fit interval yields just a few per cent change in the values of x_0 and k_{eff} . However, there is an experimentally observed abnormality in the thrust stand behavior, which makes it difficult to accurately determine the arm displacement [see Eq. (4)] that corresponds to the firing thruster. If the damped sinusoidal function $x_{\text{fit}}(t)$, obtained from the data fit, is continued in the $-t$ direction to the moment of the thruster turning off, the extrapolated value $x_e = x_{\text{fit}}(0)$ does not match the real value x_s of the steady state displacement at thruster operation (see Fig. 6, dashed line). For an ideal weakly damped spring-mass system, there must be no mismatch between x_e and x_s . However, in reality x_e is always considerably smaller than x_s . Therefore, the customary procedure of determining the arm displacement as $x_s - x_0$ might lead to a significant overestimation of the thrust.

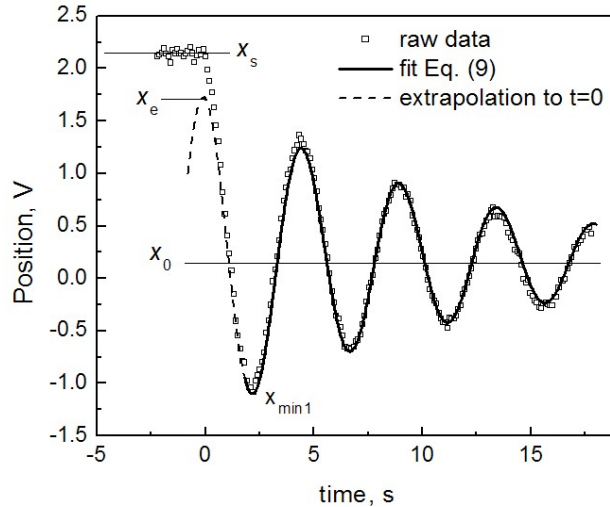


Fig. 6. Thrust arm position versus time after turning the thruster off at $t=0$. Time interval from ~ 2.4 to ~ 18 s is used for data curve fitting with the damped linear oscillator response function (solid line), Eq. (9). Note that the fit extrapolation to $t=0$ (dashed line) does not match the arm position at thruster operation: $x_e < x_s$.

A few plausible physical explanations of the observed mismatch between x_e and x_s could be proposed. One may speculate that there occurs an abrupt change in x_0 or γ during the first half period of oscillations after turning the thruster off. Another possibility is that the initial energy, stored in the stretched spring, is not entirely transferred to the energy of oscillations, but some fraction of it is lost due to surface friction or sticking between the thruster wires or gas tubes. It is worth mentioning that the same characteristic mismatch is observed without operating the thruster, if the thrust stand arm is simply moved manually away (in either $+x$ or $-x$ direction) from the equilibrium position and then released. Thus, the effect is the same for the cold and hot thrust stand. A qualitatively similar mismatch is also observed upon turning the thruster on. In any case, although the actual physical reasons of the observed non-ideal behavior of the thrust stand are not quite clear, an additional calibration of the arm displacement is required. We describe this calibration next.

B. Determination of the true displacement

An additional thrust stand calibration was performed in order to determine the true arm displacement for a given applied force. This calibration was designed so that to simulate the measurement procedure. Namely, we applied a given force to the thrust stand by suspending a calibrated weight on a thin string hanged over a low-friction pulley. To increase the calibration accuracy, the string was attached to the thrust stand arm much closer to the rotation axis than the thruster. When the arm reached a new steady state under the action of the applied force, the string was quickly burned and the arm response $x(t)$, similar to that shown in Fig. 6, was recorded. We then determined x_0 , k_{eff} , x_s , and x_e as described in Sec. IV A and compared the two limiting values of the measured force, $F_e = k_{\text{eff}}(x_e - x_0)$ and $F_s = k_{\text{eff}}(x_s - x_0)$, with the applied force. As can be seen in Fig. 7, the force F_e , which is computed using the

extrapolated position value x_e , agrees with the applied force much better than the force F_s . In fact, the discrepancy between the applied force and F_e is less than 5% of the applied force, which is smaller than the uncertainty of the measurements. From this we conclude that the true arm displacement caused by the thrust is equal to $x_e - x_0$ (see Fig. 6). This displacement was used in the data analysis to determine the thrust as

$$T = \omega_0^2 m_{\text{eff}} (x_e - x_0). \quad (10)$$

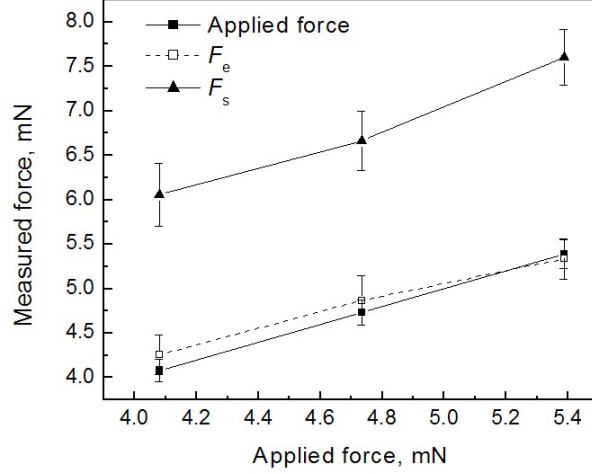


Fig. 7. Comparison of the applied calibrating force with the two limiting values of the measured force, $F_e = k_{\text{eff}}(x_e - x_0)$ and $F_s = k_{\text{eff}}(x_s - x_0)$. The uncertainty in the applied force (about $\pm 3\%$) is due to the friction in the pulley. The error bars of F_e and F_s represent the standard deviations of the data spread.

It is important to analyze the following subtlety associated with the primary calibration procedure described in Sec. III A. If the mismatch between x_s and x_e was, in fact, caused by some energy loss due to surface friction or sticking between the wires, then the same physical processes would affect the thrust arm response to the calibrating pendulum strike. We did not observe any signature of an abrupt change in the spring-mass oscillator parameters in the calibration traces $x(t)$ [see Fig. 4(a)]. Nonetheless, if some dissipative processes came into play during the energy transfer from the calibrating pendulum to the thrust stand arm, the primary calibration procedure would lead to an underestimation of V_0 and the corresponding overestimation of m_{eff} . The decrease in m_{eff} , which is required to make the measured force F_s equal to the applied force in Fig 7, is about 33%. However, the supplementary calibration (Sec. III B), which does not exploit the calibrating pendulum, gives the value of m_{eff} only about 9% smaller than the primary calibration. Therefore, the factors that cause the discrepancy between x_s and x_e seem to be unimportant for the thrust stand calibration.

C. Measurement uncertainty

It is rather difficult to estimate the uncertainty of the thrust measurements, the major reason for this being that the error of the arm displacement cannot be easily defined. Having determined that the true arm displacement is, in fact, the difference between the extrapolated position x_e and the zero level x_0 , we can ascribe the uncertainty in the displacement to the inaccuracy of the fitting and extrapolating procedure used to obtain x_e and x_0 . By varying the length and location of the data fit interval, we found that the maximum relative deviation in $x_e - x_0$ is about $\pm 5\%$. The natural frequency can be determined with the relative error of approximately $\pm 0.6\%$. Finally, as shown in Sec. III A, the uncertainty of m_{eff} is about $\pm 2.6\%$. Applying the error propagation formula to Eq. (10) yields the total relative uncertainty in thrust $\Delta T/T \lesssim \pm 6\%$. It is important to note that this estimate agrees quite well with both the observed standard deviation of the measured force F_e ($< \pm 5\%$ of F_e) and the difference between F_e and the applied calibrating force (see Fig. 7).

The thruster efficiency is defined as¹

$$\eta = \frac{T^2}{2\mu P}, \quad (11)$$

where μ is the propellant flow rate and P is the input discharge power. The relative uncertainties in μ and P are about $\pm 1.5\%$ and $\pm 1.2\%$, respectively. Thus, the efficiency is measured with about $\pm 12.2\%$ uncertainty.

V. Experimental results and discussion

The observed dependencies of the discharge current I_d , generated thrust T , and thruster efficiency η on the current in the front coil I_{front} are qualitatively similar for the 2.6 and 3 cm CHTs. In the following, we mainly show the characteristic results for one of the two thrusters. Typical dependencies of I_d and T on the current in the front coil in the 2.6 cm CHT are shown in Fig. 8. The discharge parameters are: Xenon flow rate to the anode $\mu = 4$ sccm, $I_{\text{back}} = 3$ A. The positive (negative) front coil current corresponds to the direct (cusp) magnetic field configuration (see Fig. 2).

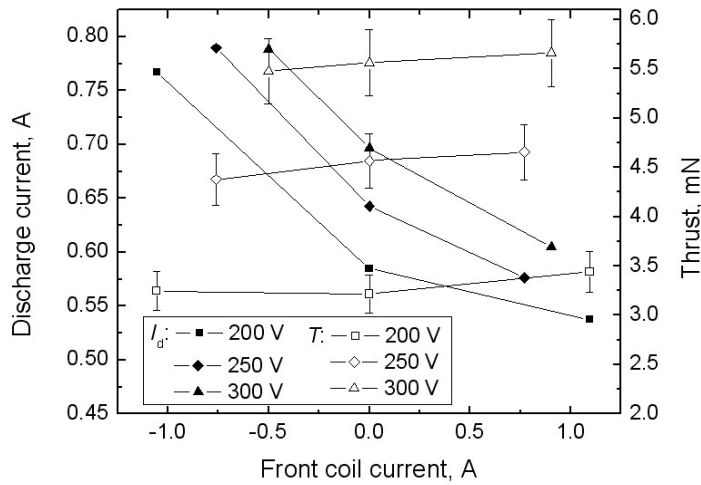


Fig. 8. The dependencies of the discharge current and thrust on the front coil current in the 2.6 cm CHT. Anode and cathode xenon flow rates are 4 sccm and 2 sccm, respectively; $I_{\text{back}} = 3$ A. $I_{\text{front}} > 0$ ($I_{\text{front}} < 0$) corresponds to the direct (cusp) magnetic field configuration.

At $I_{\text{back}} \sim 3$ A, $I_{\text{front}} \sim +1$ A minimizes the discharge current in the 2.6 cm CHT. The increase of I_{front} above this value leads to a negligible variation of the discharge current. The decrease of I_{front} , on the contrary, brings about a rather sharp increase of I_d . Along with it, as the magnetic field configuration is changed from direct to cusp, the generated thrust somewhat decreases. It should be noted, however, that the value of the front coil current that minimizes the discharge current is not universal and depends on the background gas pressure in the tank. In the experiments performed in the EPPDyL vacuum facility, the background gas pressure was typically about 5×10^{-6} Torr. In the higher background gas pressure ($\sim 5 \times 10^{-5}$ Torr) of the Small Hall Thruster facility at PPPL^{4,6}, in some of the operating regimes the discharge current is minimized by the cusp magnetic field configuration.¹¹ Interestingly, the discharge current in the 9-cm-diam. CHT, operated at the background pressure of $\sim 10^{-5}$ Torr, was always minimized in the cusp configuration.³

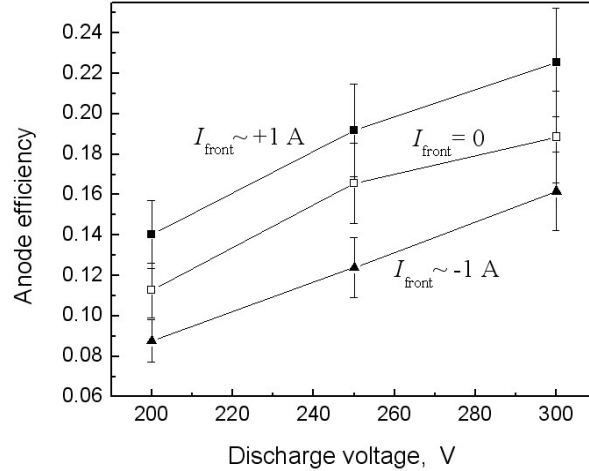


Fig. 9. The dependence of the thruster anode efficiency on the discharge voltage in the direct ($I_{\text{front}} \sim +1$ A), cusp ($I_{\text{front}} \sim -1$ A), and zero cusp ($I_{\text{front}} = 0$) magnetic field configurations of the 2.6 cm CHT. Anode and cathode xenon flows are 4 sccm and 2 sccm, respectively; $I_{\text{back}} = 3$ A.

As follows from the data shown in Fig. 8, the thruster efficiency increases with both the discharge voltage and front coil current. In Fig. 9, we show the dependence of the anode efficiency η_a (defined according to Eq. (11) with μ being the anode flow rate) on the discharge voltage with I_{front} varied as a parameter. At a given discharge voltage, the thruster efficiency increases gradually as the front coil current is varied from $I_{\text{front}} < 0$ (cusp) to $I_{\text{front}} > 0$ (direct). In the voltage range from 200 to 300 Volts, the anode efficiency in the direct configuration is approximately factor of 1.5-1.7 larger than that in the cusp configuration.

Finally, in Fig. 10 we show the dependencies of the anode efficiency and thrust on the discharge power for the 2.6 cm and 3 cm CHTs in the direct magnetic field configuration. The anode flow rate of xenon is varied between 2 sccm and 3 sccm for the 2.6 cm CHT, and between 3 sccm and 3.9 sccm for the 3 cm CHT. The cathode flow rate is constant and equal to 2 sccm. The discharge voltage is varied from 250 V to 400 V. Note that while the thrust varies substantially with power (and is almost directly proportional to P in the case of the 2.6 cm CHT), the anode efficiency remains nearly constant in the entire power range from ~ 100 W to ~ 200 W. Both thrusters can be operated with about 25% efficiency at the input power of 100 W. The degradation of the thruster performance after a few hours of continuous operation is within the measurement error.

It must be pointed out that the 3 cm CHT was also investigated independently at AFRL (Edwards AFB, CA) and at NASA Marshall Space Flight Center (Huntsville, AL). The results of the thrust measurements conducted using the VAPHER thrust stand¹² agree well with the results of the present work.¹³ This fact gives us additional confidence in the measurement technique developed herein (Sec. IV B).

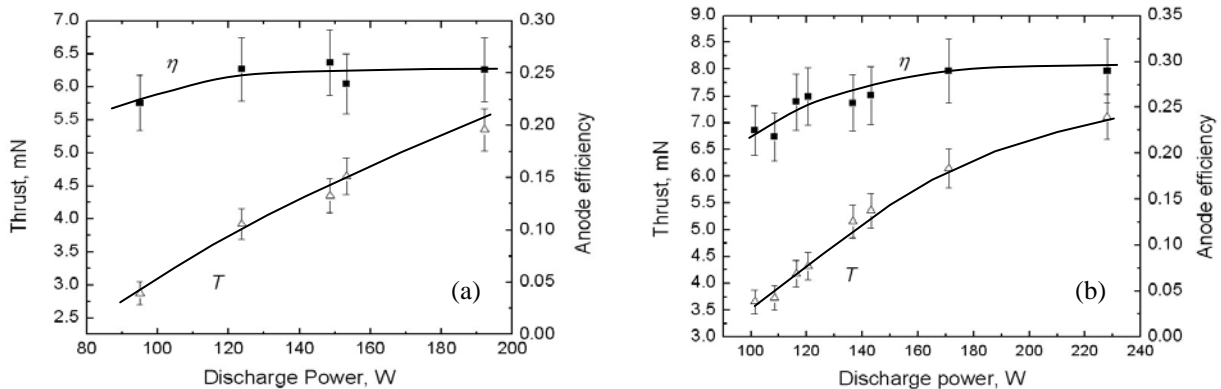


Fig. 10. The dependencies of the generated thrust and anode efficiency on the input discharge power for the 2.6 cm (a) and 3 cm CHTs.

The data trends shown in Figs 8 and 9 can be interpreted in the following manner. The fact that the discharge current decreases with the increase in I_{front} implies that the electron transport to the anode is suppressed more strongly in the direct magnetic field configuration than in the cusp configuration (see Fig. 2). The slight increase of the thrust in the direct configuration is, most likely, a manifestation of a better ion flux focusing. Detailed plasma potential measurements inside the CHT channel similar to those performed in Ref. 6 are required in order to explain how exactly the plasma responds to the variation of the magnetic field distribution. Studying the variation of the internal plasma parameters with the magnetic field is a subject of ongoing research.

The efficiency of the cylindrical thrusters at 100 W power level, $\eta_a \sim 22\%$, is comparable to and in some cases larger than that of the state-of-the-art conventional annular low-power thrusters, such as BHT-200-X2B ($\eta_a \sim 21\%$),¹⁴ SPT-30 ($\eta_a \sim 22\%$),¹⁵ KM-37 ($\eta_{\text{tot}} \sim 24\%$),¹⁶ KM-20M ($\eta_{\text{tot}} < 30\%$),^{17,18} and MIT HT ($\eta_{\text{tot}} \sim 6\%$).¹⁹ However, the cylindrical thrusters are likely to have a very important advantage over the annular design thrusters, namely, a longer lifetime. Yet another thruster that may improve on certain design issues associated the channel erosion and magnetic circuit miniaturization, is a linear Hall thruster of Ref. 20. However, the electron drift in linear thrusters terminates on the channel walls. The advantage of a large Hall parameter, which leads to a smaller electron current, is lost and the thruster efficiency tends to be relatively low, $\eta_a \sim 9\%$ at $P = 100$ W.

VI. Conclusions

Scaling to low-power Hall thrusters requires the thruster channel to be scaled down, while the magnetic field must be increased inversely with the scaling parameter. The conventional annular design of Hall thrusters has an unfavorable surface-to-volume ratio at small size. Thus, it is not surprising that low power operation of annular Hall thrusters is problematic: The efficiency tends to be lower, and the lifetime issues are more aggravated. An alternative approach, which may be more suitable for scaling to low power, is a CHT. Ion acceleration in CHTs occurs mainly in the cylindrical part of the channel and beyond the thruster exit. Therefore, the CHT, having lower surface-to-volume ratio as compared with conventional Hall thrusters, should suffer lower erosion of the channel walls and have a longer lifetime. In contrast to the conventional geometry, in the cylindrical geometry the axial potential distribution is critical for electron confinement in the discharge.

In the present work we investigated the effect of the magnetic field on the performance of the low-power CHTs with outer channel diameters of 2.6 cm and 3 cm. Specifically, two magnetic field configurations, which correspond to different polarities of the currents in the thruster electromagnets, were compared: 1) “cusp” configuration with the enhanced radial component of the magnetic field in the cylindrical part of the channel (counter-directed currents) and 2) “direct” configuration with the enhanced axial field component and stronger magnetic mirror in the cylindrical part of the channel (co-directed currents).

The EPPDyL thrust stand was used for the thrust measurements. Three independent calibrating techniques were employed in order to analyze the thrust stand dynamics at low applied thrust. To accommodate the thermal drift, caused by the thruster operation, as well as the observed abnormality in the thrust stand behavior, associated with turning on or off the applied force, a special measurement procedure was designed. With the developed procedure, the uncertainty of thrust measurements was show to be equal to about $\pm 6\%$.

The experimental results have demonstrated a substantial flexibility in the thruster magnetic field configuration, which is a key tool in achieving the high-efficiency operation. The electron confinement and ion acceleration can be optimized over a family of realizable magnetic field distributions. The optimal regimes of thruster operation at low background pressure (below 10^{-5} Torr) appear to be different from those at higher pressure ($\sim 5 \times 10^{-5}$ Torr). At low background gas pressure, for both the 2.6 cm and 3 cm CHTs the discharge current decreases and the generated thrust slightly increases as the magnetic field configuration is changed from cusp to direct. This implies that the electron transport to the anode is suppressed more strongly, and the directionality of ion acceleration is likely better in the direct magnetic field configuration than in the cusp configuration. The thruster efficiency is accordingly larger in the direct configuration. In the power range 100 – 200 W, the anode efficiency of the 2.6 cm CHT is almost constant and equal to about 25%, while for the 3 cm CHT it varies from $\sim 25\%$ to $\sim 30\%$. Thus, the anode efficiency of the CHTs (in the direct configuration) is comparable to and in some cases larger than that of the state-of-the-art conventional annular low-power thrusters. However, CHTs, having lower surface-to-volume ratio as compared with conventional annular design Hall thrusters, should suffer lower erosion of the channel walls and, therefore, have a longer lifetime.

Acknowledgments

The authors are grateful to Professor Edgar Choueiri for the provided opportunity to work with the EPPDyL thrust stand, and to Mr. Robert Sorenson for his assistance in the thrust measurements. This work was supported by grants from AFOSR, DARPA, and USDOE Contract AC02-76CH0-3073.

References

- ¹A.I. Morozov and V.V. Savelyev, in *Review of Plasma Physics*, edited by B.B. Kadomtsev and V.D. Shafranov (Consultants Bureau, New York, 2000), Vol. 21, p. 203.
- ²J. Mueller, in *Micropropulsion for Small Spacecraft*, edited by M.M. Micci and A.D. Ketsdever (AIAA Progress in Astronautics and Aeronautics, 2000), Vol. 187, p. 45.
- ³Y. Raitses and N.J. Fisch, "Parametric investigations of a nonconventional Hall thruster", *Phys. Plasmas*, vol. 8, no. 5, pp. 2579-2586, 2001.
- ⁴A. Smirnov, Y. Raitses, and N.J. Fisch, "Parametric investigation of miniaturized cylindrical and annular Hall thrusters", *J. Appl. Phys.*, vol. 92, no. 10, pp. 5673-5679, 2002.
- ⁵A. Smirnov, Y. Raitses, and N.J. Fisch, "Enhanced ionization in the cylindrical Hall thruster", *J. Appl. Phys.*, vol. 94, no. 2, pp. 852-857, 2003.
- ⁶A. Smirnov, Y. Raitses, and N.J. Fisch, "Plasma measurements in a 100 W cylindrical Hall thruster", *J. Appl. Phys.*, vol. 95, no.5, pp. 2283-2292, 2004.
- ⁷A. Smirnov, Y. Raitses, and N.J. Fisch, "Electron cross-field transport in a low power cylindrical Hall thruster", *Phys. Plasmas*, vol. 11, no. 11, 4922-4933, 2004.
- ⁸Y. Raitses, A. Smirnov, and N.J. Fisch, "Cylindrical Hall thrusters", presented at the 15th Annual NASA/JPL/MSFC Advanced Space Propulsion Workshop, Pasadena, CA, 2004.
- ⁹E. A. Cubbin, J. K. Ziemer, E. Y. Choueiri, and R. G. Jahn, "Pulsed thrust measurements using laser interferometry", *Rev. Sci. Instrum.*, vol. 68, no. 6, pp. 2339-2346, 1997.
- ¹⁰S.G. Rabinovich, *Measurement errors : theory and practice*, p. 47. New York: American Institute of Physics, 1995.
- ¹¹A. Smirnov, Y. Raitses, and N.J. Fisch, "Electron cross-field transport in a miniaturized cylindrical Hall thruster" submitted to IEEE Transactions on Plasma Science in September 2005.
- ¹²T.E. Markusic, J.E. Jones, and M.D. Cox. "Thrust stand for electric propulsion performance evaluation", 40th AIAA/ASME/SAE/ASEE Joint Propulsion Conference, Ft. Lauderdale, FL, 2004, AIAA-2004-3441.
- ¹³K.A. Polzin, T.E. Markusic, B.J. Stanojev, A. Dehoyos, Y. Raitses, A. Smirnov, and N.J. Fisch, "Performance of a low-power cylindrical Hall thruster", IEPC paper 2005-011, to be presented at the 28th International Electric Propulsion Conference, Princeton, NJ, October 2005.
- ¹⁴V. Hruby, J. Monheiser, B. Pote, C. Freeman, and W. Connolly, IEPC paper 99-092, 26th International Electric Propulsion Conference, Kitakyushu, Japan, June 1999.
- ¹⁵D. Jacobson and R. Jankovsky, AIAA paper 98-3792, 34th Joint Propulsion Conference, Cleveland, OH, July 1998.
- ¹⁶M.B. Belikov, O.A. Gorshkov, V.A. Muravlev, R.N. Rizakhanov, A.A. Shagayda, and A.U. Shnirev, AIAA paper 2001-3780, 37th Joint Propulsion Conference, July 2001.
- ¹⁷A.I. Bugrova, A.D. Desiatskov, H.R. Kaufman, V.K. Kharchevnikov, A.I. Morozov, and V.V. Zhurin, IEPC paper 01-344-2, 27th International Electric propulsion Conference, Pasadena, California October 14-19, 2001.
- ¹⁸A.I. Bugrova, A.D. Desiatskov, H.R. Kaufman, V.K. Kharchevnikov, A.I. Morozov, and V.V. Zhurin, IEPC paper 03-0263, *Proceedings of the 28th International Electric Propulsion Conference, Toulouse, France* (Electric Rocket Propulsion Society, Cleveland, OH, 2003).
- ¹⁹V. Khayms and M. Martinez-Sanches, in *Micropropulsion for Small Spacecraft*, edited by M.M. Micci and A.D. Ketsdever (AIAA Progress in Astronautics and Aeronautics, 2000), Vol. 187, p. 45.
- ²⁰D. P. Schmidt, N. B. Meezan, W. A. Hargus Jr and M. A. Cappelli, "A low-power, linear-geometry Hall plasma source with an open electron-drift", *Plasma Sources Science and Technology*, 9, 2000, pp.68-76.